

## Detection of extended X-ray emission around the PeVatron microquasar V4641 Sgr with XRISM

HIROMASA SUZUKI,<sup>1</sup> NAOMI TSUJI,<sup>2,3</sup> YOSHIAKI KANEMARU,<sup>1</sup> MEGUMI SHIDATSU,<sup>4</sup> LAURA OLIVERA-NIETO,<sup>5</sup>  
SAMAR SAFI-HARB,<sup>6</sup> SHIGEO S. KIMURA,<sup>7,8</sup> EDUARDO DE LA FUENTE,<sup>9</sup> SABRINA CASANOVA,<sup>10</sup> KAYA MORI,<sup>11</sup>  
XIAOJIE WANG,<sup>12</sup> SEI KATO,<sup>13,14</sup> DAI TATEISHI,<sup>15</sup> HIDEKI UCHIYAMA,<sup>16</sup> TAKAAKI TANAKA,<sup>17</sup> HIROYUKI UCHIDA,<sup>18</sup>  
SHUN INOUE,<sup>18</sup> DEZHI HUANG,<sup>19</sup> MARIANNE LEMOINE-GOUMARD,<sup>20</sup> DAIKI MIURA,<sup>15,1</sup> SHOJI OGAWA,<sup>1</sup>  
SHOGO B. KOBAYASHI,<sup>21</sup> CHRIS DONE,<sup>22</sup> MAXIME PARRA,<sup>23,24</sup> MARIA DÍAZ TRIGO,<sup>25</sup> TEO MUÑOZ-DARIAS,<sup>26,27</sup>  
MONTERRAT ARMAS PADILLA,<sup>26,27</sup> RYOTA TOMARU,<sup>28</sup> AND YOSHIHIRO UEDA<sup>29</sup>

<sup>1</sup>*Institute of Space and Astronautical Science (ISAS), Japan Aerospace Exploration Agency (JAXA), Kanagawa 252-5210, Japan*

<sup>2</sup>*Faculty of Science, Kanagawa University, 3-27-1 Rokukakubashi, Kanagawa-ku, Yokohama-shi, Kanagawa 221-8686, Japan*

<sup>3</sup>*Interdisciplinary Theoretical & Mathematical Science Program (iTHEMS), RIKEN, 2-1 Hirosawa, Wako, Saitama 351-0198, Japan*

<sup>4</sup>*Department of Physics, Ehime University, 2-5 Bunkyocho, Matsuyama, Ehime 790-8577, Japan*

<sup>5</sup>*Max-Planck-Institut für Kernphysik, P.O. Box 103980, D 69029 Heidelberg, Germany*

<sup>6</sup>*Department of Physics and Astronomy, University of Manitoba, Winnipeg, MB R3T 2N2, Canada*

<sup>7</sup>*Frontier Research Institute for Interdisciplinary Sciences, Tohoku University, Sendai 980-8578, Japan*

<sup>8</sup>*Astronomical Institute, Graduate School of Science, Tohoku University, Sendai 980-8578, Japan*

<sup>9</sup>*Departamento de Física, CUCEI, Universidad de Guadalajara, Blvd. Marcelino García Barragán 1420, Olímpica, 44430, Guadalajara, Jalisco, México*

<sup>10</sup>*Instytut Fizyki Jądrowej PAN, ul. Radzikowskiego 152, 31-342 Kraków, Poland*

<sup>11</sup>*Columbia Astrophysics Laboratory, Columbia University, 538 West 120th Street, New York, NY 10027, USA*

<sup>12</sup>*Department of Physics, Michigan Technological University, Houghton, MI, USA*

<sup>13</sup>*Institute for Cosmic Ray Research, University of Tokyo, Kashiwa 277-8582, Japan*

<sup>14</sup>*Institut d'Astrophysique de Paris, CNRS UMR 7095, Sorbonne Université, 98 bis bd Arago 75014, Paris, France (Present affiliation)*

<sup>15</sup>*Department of Physics, Graduate School of Science, The University of Tokyo, 7-3-1 Hongo, Bunkyo-ku, Tokyo 113-0033, Japan*

<sup>16</sup>*Faculty of Education, Shizuoka University, 836 Ohya, Suruga-ku, Shizuoka, Shizuoka, 422-8529, Japan*

<sup>17</sup>*Konan University, Department of Physics, 8-9-1 Okamoto, Higashinada, Kobe, Hyogo, Japan, 658-8501*

<sup>18</sup>*Department of Physics, Graduate School of Science, Kyoto University, Kitashirakawa Oiwake-cho, Sakyo-ku, Kyoto 606-8502, Japan*

<sup>19</sup>*Department of Physics, University of Maryland, College Park, MD, USA*

<sup>20</sup>*Université Bordeaux, CNRS, CENBG, UMR 5797, F-33170 Gradignan, France*

<sup>21</sup>*Department of Physics, Tokyo University of Science, 1-3 Kagurazaka, Shinjuku-ku, Tokyo 162-8601, Japan*

<sup>22</sup>*Centre for Extragalactic Astronomy, Department of Physics, University of Durham, South Road, Durham DH1 3LE, UK*

<sup>23</sup>*Université Grenoble Alpes, CNRS, IPAG, 38000 Grenoble, France*

<sup>24</sup>*Dipartimento di Matematica e Fisica, Università degli Studi Roma Tre, Via della Vasca Navale 84, 00146 Roma, Italy*

<sup>25</sup>*ESO, Karl-Schwarzschild-Strasse 2, 85748, Garching bei München, Germany*

<sup>26</sup>*Instituto de Astrofísica de Canarias, E-38205 La Laguna, Tenerife, Spain*

<sup>27</sup>*Departamento de Astrofísica, Universidad de La Laguna, E-38206 La Laguna, Tenerife, Spain*

<sup>28</sup>*Department of Earth and Space Science, Graduate School of Science, Osaka University, 1-1 Machikaneyama, Toyonaka, Osaka 560-0043, Japan*

<sup>29</sup>*Department of Astronomy, Kyoto University, Kitashirakawa-Oiwake-cho, Sakyo-ku, Kyoto, Kyoto 606-8502, Japan*

### ABSTRACT

A recent report on the detection of very-high-energy gamma rays from V4641 Sagittarii (V4641 Sgr) up to  $\approx 0.8$  peta-electronvolt has made it the second confirmed “PeVatron” microquasar. Here we report on the observation of V4641 Sgr with X-Ray Imaging and Spectroscopy Mission (XRISM) in September 2024. Thanks to the large field of view and low background, the CCD imager Xtend successfully detected for the first time X-ray extended emission around V4641 Sgr with a significance of  $\gtrsim 4.5\sigma$  and  $> 10\sigma$  based on our imaging and spectral analysis, respectively. The spatial extent is estimated to have a radius of  $7 \pm 3$  arcmin ( $13 \pm 5$  pc at a distance of 6.2 kpc) assuming a Gaussian-like radial distribution, which suggests that the particle acceleration site is within  $\sim 10$  pc of the microquasar. If the X-ray morphology traces the diffusion of accelerated electrons, this spatial extent can be explained by either an enhanced magnetic field ( $\sim 80 \mu\text{G}$ ) or a suppressed diffusion coefficient ( $\sim 10^{27} \text{ cm}^2 \text{ s}^{-1}$  at 100 TeV). The integrated X-ray flux,  $(4\text{--}6) \times 10^{-12} \text{ erg s}^{-1} \text{ cm}^{-2}$  (2–10 keV),

would require a magnetic field strength higher than the galactic mean ( $\gtrsim 8 \mu\text{G}$ ) if the diffuse X-ray emission originates from synchrotron radiation and the gamma-ray emission is predominantly hadronic. If the X-rays are of thermal origin, the measured extension, temperature, and plasma density can be explained by a jet with a luminosity of  $\sim 2 \times 10^{39} \text{ erg s}^{-1}$ , which is comparable to the Eddington luminosity of this system.

*Keywords:* Low-mass x-ray binary stars (939) — Gamma-ray sources (633) — Radio jets (1347) — Non-thermal radiation sources (1119)

## 1. INTRODUCTION

The origin of Galactic cosmic rays has been a long-standing question and is of increasing interest in recent years thanks to the growing high-sensitivity X-ray, gamma-ray, and neutrino observatories. Among the candidates for Galactic cosmic-ray accelerators, microquasars, where accreting black holes are powering jets, are an emerging class of Galactic PeVatrons after the tera-electronvolt (TeV) detection of the W50-SS 433 system (Abeysekera et al. 2018; H. E. S. S. Collaboration et al. 2024). Most recently, LHAASO discovered gamma-ray emission exceeding 100 TeV from directions overlapping with several microquasars (LHAASO Collaboration 2024). The detection of gamma rays with  $E > 100 \text{ TeV}$  suggests that parent particles (either protons or electrons) are accelerated beyond 1 PeV, indicating these microquasars are potential PeVatrons.

V4641 Sagittarii (V4641 Sgr) was found to exhibit extended gamma-ray emission up to  $\approx 0.8$  peta-electronvolt (PeV) in its surroundings, which is the brightest among the TeV-detected microquasars (Alfaro et al. 2024; LHAASO Collaboration 2024). V4641 Sgr is a low-mass X-ray binary (LMXB) consisting of a black hole with a mass of  $6.4 \pm 0.6 M_{\odot}$  and a B9III companion star with a mass of  $2.9 \pm 0.4 M_{\odot}$  (MacDonald et al. 2014), located at a distance of  $\approx 6.2 \text{ kpc}$  (MacDonald et al. 2014; Gandhi et al. 2019). In contrast to other microquasars, V4641 Sgr is characterized by violent X-ray outbursts, which include a rapid onset and exponential decay (Revnivtsev et al. 2002). The outbursts are observed once in  $\sim 2$  years without clear periodicity<sup>1</sup>. Radio observations with the Very Large Array, performed within one day after an X-ray burst in 1999, showed a luminous jet-like radio structure of about  $0''.25$  length (Hjellming et al. 2000), much more compact than the gamma-ray extension of  $\approx 0''.54$  (Alfaro et al. 2024).

In these months, V4641 Sgr is gaining even more attention because it has been exhibiting a bursting activity

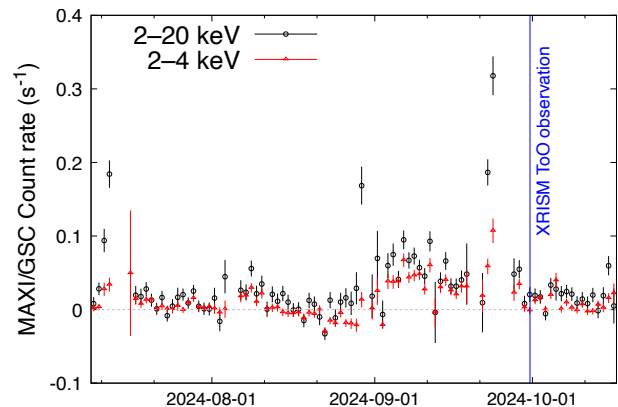


**Figure 1.** MAXI/GSC light curves of V4641 Sgr showing the bursting activity in September 2024, obtained from [http://maxi.riken.jp/star\\_data/J1819-254/J1819-254.html](http://maxi.riken.jp/star_data/J1819-254/J1819-254.html). The observation period with XRISM is indicated with the blue transparent region.

since September 2024 (Figure 1; report on MAXI/GSC observations: <https://www.astronomerstelegam.org/?read=16804>). Following other X-ray observatories such as Swift and XMM-Newton, the X-Ray Imaging and Spectroscopy Mission (XRISM; Tashiro et al. 2018, 2020; Tashiro et al. 2024) observed V4641 Sgr as a generic Target of Opportunity (ToO) observation. In this paper, we report on a morphological and spectral analysis of the environment of V4641 Sgr and the detection of extended emission with XRISM.

## 2. OBSERVATION AND DATA REDUCTION

XRISM is equipped with the microcalorimeter Resolve (Ishisaki et al. 2018) and wide field-of-view (FoV) CCD camera Xtend (Mori et al. 2022). In this work, we focus on the data obtained with Xtend to search for a possible extended emission.<sup>2</sup> Xtend provides a  $\approx 38' \times 38'$  FoV for the energy range 0.4–13 keV with an energy resolution better than 200 eV (FWHM: full width half

<sup>1</sup> Refer to, e.g., a light curve by MAXI ([http://maxi.riken.jp/star\\_data/J1819-254/J1819-254.html](http://maxi.riken.jp/star_data/J1819-254/J1819-254.html)).

<sup>2</sup> The results of the high-resolution spectroscopy of V4641 Sgr itself with Resolve will be reported separately (Shidatsu et al., in prep.).

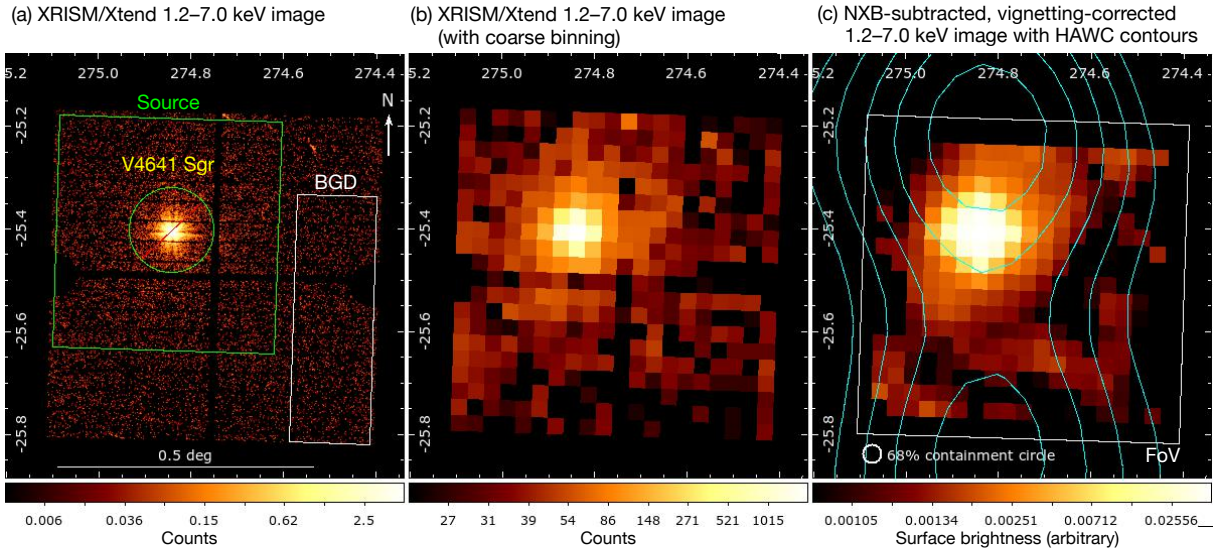


**Figure 2.** (a) A 1.2–7.0 keV XRISM Xtend image with the regions for the spectral analysis. (b) Same with a course binning. (c) The image after the particle-background subtraction and vignetting correction and with the HAWC gamma-ray contours ( $> 1$  TeV; Alfaro et al. 2024) and the Xtend field of view (FoV) overlaid. The 68% containment circle of the point spread function at 6.4 keV is shown as a reference. The images are shown on the Equatorial coordinates (J2000).

maximum; Mori et al. 2024). The angular resolution is  $< 1'.7$  (HPD: half power diameter; Tamura et al. 2024).

V4641 Sgr was observed with XRISM as a generic ToO target on September 30, 2024 UT (ObsID: 901001010). Since the allocated time for generic ToO observations is very limited, the observation duration was only  $\approx 20$  ks. We reduced the data with the pre-release Build 7 XRISM software with HEASoft ver. 6.32 (HEASARC 2014) and calibration database (CALDB) ver. 8 (v20240815) (Terada et al. 2021; Loewenstein et al. 2020). We excluded periods of the Earth eclipse and sunlit Earth’s limb, as well as passages of the South Atlantic Anomaly. The effective exposure of Xtend that remains after the standard data reduction is  $\approx 12.2$  ks. We removed flickering pixels<sup>3</sup> using the `searchflickpix` tool in addition to removing bad pixels and columns manually.

For the morphological analysis, we use the night-earth and day-earth occultation data collected from March 10 to July 31, 2024 from the XRISM trend archive (Rev. 3).<sup>4</sup> The night-earth data are used to evaluate the event rate and spatial distribution of the particle background (Non-X-ray background), whereas the day-earth data are used as a reference for the detector image from a uniform emission on the plane of the sky, which allows us to obtain the vignetting curve (effective area as a function of the off-axis angle).

<sup>3</sup> Pixels with anomalously high event rates, which mostly record pseudo events at  $\lesssim 1$  keV (Nakajima et al. 2018).

<sup>4</sup> <https://data.darts.isas.jaxa.jp/pub/xrism/data/trend/rev3/>

In our spectral analysis, we use XSPEC ver. 12.13.1 (Arnaud 1996) with the *C*-statistic (Cash 1979), and AtomDB ver. 3.0.9 (Foster et al. 2012). Redistribution Matrix Files (RMFs) are created with the `xtdrmf` task using the cleaned event file and CALDB based on ground measurements. Auxiliary Response Files (ARFs) are generated with the `xaarfgen` task assuming constant surface-brightness emission because the sky background dominates the data. The errors given in the text and figures indicate  $1\sigma$  confidence intervals.

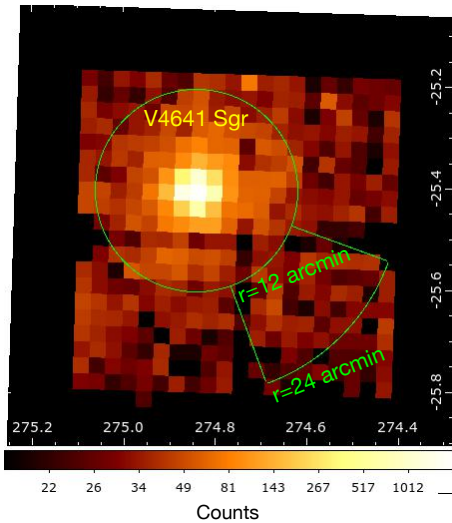
### 3. ANALYSIS AND RESULTS

#### 3.1. X-ray morphology

Figure 2 (a) and (b) show a 1.2–7.0 keV image with XRISM Xtend, indicating a hint of extended emission around V4641 Sgr. Here, events with lower and higher energies are excluded because of the significant contribution of the sky and particle background, respectively (see Section 3.2). To be more precise, we subtract the particle-background image extracted from the night-earth dataset and scaled to match the 9.0–13.0 keV event rate, dominated by the particle background, of the V4641 Sgr observation. Then we also correct for the vignetting of the mirror assembly using the day-earth image. As a result, we obtain Figure 2 (c), which shows extended emission around V4641 Sgr.

In order to quantify the spatial extent of the extended emission, we extract a one-dimensional radial profile centered at V4641 Sgr (Figure 3). The profile is extracted from a circle with a radius of 12 arcmin and from a partial annulus extending from 12 to 24 arcmin (Fig-

(a) XRISM/Xtend 1.2–7.0 keV image with radial-profile extraction region



(b) 1.2–7.0 keV radial profile and best-fit models

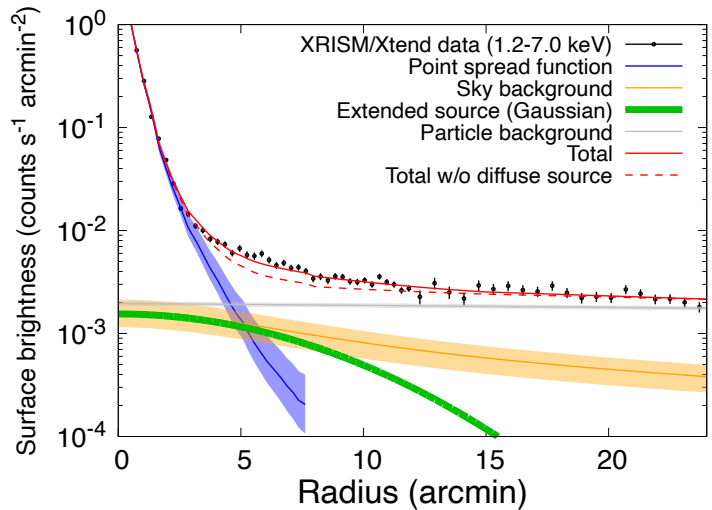


**Figure 3.** (a) A 1.2–7.0 keV XRISM Xtend image with the radial-profile extraction region centered at V4641 Sgr (green). (b) Extracted radial profile with the models for the point spread function at 6.4 keV, sky background, particle background, and extended emission modeled with a Gaussian function. The transparent regions indicate the systematic uncertainty ranges (see text for details).

ure 3 (a)). The location of the partial annulus is chosen to extend to the region where events are dominated by particle background. The radial profile for the emission of V4641 Sgr (point spread function: PSF) is made with a ray-tracing simulation using the `xrtraytrace` task at 6–7 keV<sup>5</sup>. The morphology of the sky background, which should originate from a nearly uniform emission on the plane of the sky, is modeled using the day-earth image, which is equivalent to the vignetting image. The radial profile of the particle-background is extracted from the night-earth dataset. As for the extended emission, we assume a Gaussian-like distribution as a simple model. We model the radial profile from the 1.2–7.0 keV image with the empirical model “(V4641 Sgr) + (extended emission) + (sky background) + (particle background)”. The free parameters include the normalizations of the components of V4641 Sgr, the extended emission, and sky background, and the width of the extended emission (Gaussian function). We employ a least chi-square fit to determine the best-fit parameters and their confidence intervals. The best-fit model is shown in Figure 3 (b). We obtain the best-fit Gaussian sigma of the extended-emission model of  $7 \pm 3$  arcmin, which is converted to  $13 \pm 5$  pc at a distance of 6.2 kpc. The model without the extended emission does

<sup>5</sup> The in-orbit calibration of the PSF has been done best for this energy range. The energy dependence of the PSF in 1.2–7.0 keV ( $< 80\%$  at radii smaller than 8 arcmin: Tamura et al. 2022) is included in the systematic uncertainty considered later.

not fit the data in the radii of  $\approx 5$ –12 arcmin (Figure 3 (b)). The detection significance can be evaluated from the fit statistics with and without the extended-emission model using the F-test, to be  $\gtrsim 4.5\sigma$  (F-test probability  $\lesssim 8.8 \times 10^{-6}$ ) taking into account the upper limits of the systematic uncertainties described below.

We evaluate the impact of the systematic uncertainties associated with the PSF tail:  $< 80\%$  within the radii  $< 8$  arcmin (Tamura et al. 2022; Tamura et al. 2024), off-axis effective area:  $< 30\%$ , and particle background level:  $< 5\%$  (Uchida et al., in prep.). These uncertainty levels are also shown in Figure 3 (b). These systematic uncertainties can alter the flux of the emission up to  $\approx 30\%$ .

### 3.2. X-ray spectra

In the next step, we examine the X-ray spectrum of the extended emission marginally detected in Section 3.1. The source and background (BGD) regions are defined as shown in Figure 2 (a). The source region encloses most of the apparent extended emission (Section 3.1) but without the contribution of V4641 Sgr itself<sup>6</sup>. The BGD region is nearly free from the extended emission (Figure 2 (c)). We only use the energies above 1.0 keV, where the contamination from potential flickering pixels and bad pixels remaining after data reduction is negligible.

<sup>6</sup>  $\lesssim 3\%$  of the total flux remains within the source region (Tamura et al. 2024), which is lower than the sky background level.

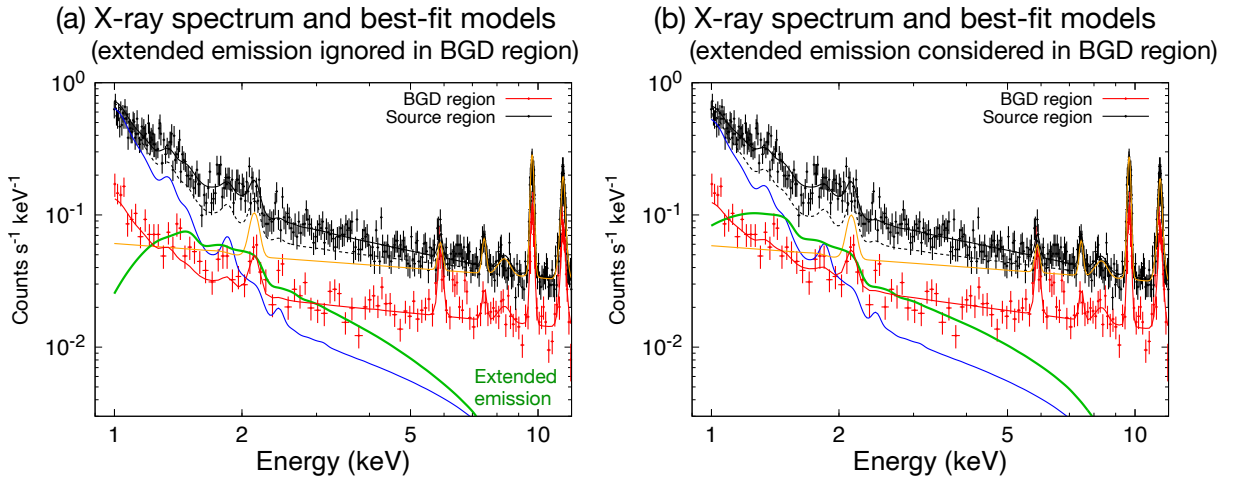


**Figure 4.** (a) X-ray spectra obtained with XRISM Xtend and the best-fit spectral models in the case where contamination of the extended emission in the BGD region is ignored and (b) assumed to be 10% in flux of the source region. The green, blue, and orange solid lines indicate the extended emission, sky background, and particle background, respectively, for the source region. The black and red solid lines indicate the total models for the source and BGD regions, respectively. The black dashed line is the total model for the source region but without the extended-emission component.

For the spectral model, we consider the sky and particle background in addition to the extended source. As for the sky background, we apply the foreground emission (Local Hot Bubble), Milky Way Halo (Transabsorption emission) and Cosmic X-ray Background (CXB). The former two are modeled with the `apec` model in XSPEC with the electron temperatures of 0.1 keV and 0.6 keV, respectively, and the solar abundance (Kuntz & Snowden 2008; Masui et al. 2009; Yeung et al. 2024). The uncertain Galactic absorption for the Milky Way Halo component is not considered because it does not strongly affect the energy range we focus on. Only their fluxes are treated as free parameters. As for CXB, we use the `powerlaw` model with a photon index of 1.41 and the 2–10 keV flux fixed to  $5.4 \times 10^{-15}$  erg cm $^{-2}$  arcmin $^{-2}$  (Kushino et al. 2002). The Galactic absorption is considered with the `tbabs` model with a column density of  $1.6 \times 10^{21}$  cm $^{-2}$  (Wilms et al. 2000; HI4PI Collaboration et al. 2016).

The particle background model is developed from the night-earth observation data. The extracted spectrum can be explained with a model composed of the fluorescence lines of Au-M, Ni-K, and Au-L and a continuum (`powerlaw`) (Nakajima et al. 2018; Uchida et al. in prep.). As the particle background level depends on the satellite position and solar activity but without changing the spectral shape significantly ( $\lesssim 10\%$ ; Uchida et al. in prep.), we apply this spectral model to the V4641 Sgr observation. Only the total normalization is treated as a free parameter.

As for the extended emission, we first use an absorbed power-law model (`tbabs` $\times$ `powerlaw`). In the spectral modeling, we fit the spectra of the source and BGD si-

multaneously with two assumptions: (a) the extended emission does not contaminate the BGD region and (b) 10% flux of the extended emission in the source region contributes to the BGD region. The contamination level of 10% is derived by evaluating the integrals of a Gaussian function for the extended source, assuming a sigma of 10 arcmin (best-fit value plus  $1\sigma$  error; see Section 3.1) over the source and BGD regions. In the spectral modeling, we find that the detector gain is slightly shifted from that expected by the RMFs due to the degradation on orbit in  $\sim 1$  year. We thus correct the gain slopes of the RMFs by  $\approx 0.3\%$  and  $\approx 0.2\%$  for the source and BGD regions, respectively, to fit the detector background lines.

Figure 4 shows the results corresponding to the two cases (a) and (b). We obtain the fit statistics  $C$ -stat/d.o.f. = 4190.1/3658 and 4147.6/3658, respectively. The case (b) better explains the observations. The best-fit spectral parameters of the extended emission are summarized in Table 1. The unabsorbed flux in 2–10 keV is determined to be  $\approx 7$ – $10 \times 10^{-15}$  erg s $^{-1}$  cm $^{-2}$  arcmin $^{-2}$ . The spectral index is found to depend on the assumptions strongly, and thus is not constrained well. The detection significance of the extended emission can be evaluated from the fit statistics with and without the extend-emission model using the likelihood ratio test (for the  $C$ -statistic), to be  $> 10\sigma$  ( $\Delta C = 361.9$  and  $\Delta$ d.o.f. = 3).

To account for the possibility that the emission is of thermal origin, we also assume a thermal emission model (case (c)). If a collisional ionization equilibrium plasma model (`apec`) with the solar abundance (Wilms et al. 2000) and with free electron temperature and normal-

ization replaces the power-law model of the case (a), we obtain the fit statistics  $C\text{-stat}/\text{d.o.f.} = 4192.3/3658$ . This is similar to the result of the case (a). The derived parameters are shown in Table 1. The electron temperature  $kT_e$  is constrained to be  $3.2 \pm 0.7$  keV. The unabsorbed flux in 2–10 keV is estimated to be  $(7 \pm 1) \times 10^{-15}$  erg s $^{-1}$  cm $^{-2}$  arcmin $^{-2}$ . Based on the volume emission measure  $n_e n_p V$ , where the  $n_e$ ,  $n_p$ , and  $V$  respectively are the electron and proton density, and volume, one can derive the plasma density  $\approx 0.3$  cm $^{-3}$  ( $r/10$  pc) $^{-1.5}$ , with the  $r$  being the radius of the spherical plasma.

**Table 1.** Best-fit spectral parameters of the extended emission.

Case (a)	$N_H$ ( $10^{22}$ cm $^{-2}$ )	$1.8 \pm 0.5$
	Power-law index	$2.4 \pm 0.3$
	Power-law flux (2–10 keV) ( $10^{-15}$ erg s $^{-1}$ cm $^{-2}$ arcmin $^{-2}$ )	$7.8 \pm 0.9$
	Integrated power-law flux (2–10 keV) <sup>a</sup> ( $10^{-12}$ erg s $^{-1}$ cm $^{-2}$ )	$4.3 \pm 0.5$
	$C\text{-stat.}/\text{d.o.f.}$	4190.1/3658
Case (b)	$N_H$ ( $10^{22}$ cm $^{-2}$ )	$0.6 \pm 0.4$
	Power-law index	$1.8 \pm 0.2$
	Power-law flux (2–10 keV) ( $10^{-15}$ erg s $^{-1}$ cm $^{-2}$ arcmin $^{-2}$ )	$9.2 \pm 1.1$
	Integrated power-law flux (2–10 keV) <sup>a</sup> ( $10^{-12}$ erg s $^{-1}$ cm $^{-2}$ )	$5.1 \pm 0.6$
	$C\text{-stat.}/\text{d.o.f.}$	4147.6/3658
Case (c)	$N_H$ ( $10^{22}$ cm $^{-2}$ )	$1.5 \pm 0.4$
	$kT_e$ (keV)	$3.2 \pm 0.7$
	$n_e n_p V$ ( $10^{58}$ cm $^{-3}$ )	$1.3 \pm 0.2$
	$C\text{-stat.}/\text{d.o.f.}$	4192.3/3658

<sup>a</sup>Integrated flux for the source region, which has an area of 629.4 arcmin $^2$ .

Considering its location ( $\ell = 6^\circ 77$  and  $b = -4^\circ 79$ ) close to the Galactic center, the spectrum is possibly affected by the Galactic Ridge X-ray Emission (GRXE: Uchiyama et al. 2013; Yamauchi et al. 2016), but the exact contribution at such high galactic altitudes is quite uncertain. So, we add a GRXE model (with the spectral shape described in Table 3 of Uchiyama et al. 2013) with the highest flux level allowed from the best-fit radial-profile models (Section 3.1)<sup>7</sup>. As a result, the spectral excess is still found to be significant with

a  $\approx 9\sigma$  significance with a somewhat reduced flux of  $(3.6 \pm 0.8) \times 10^{-15}$  erg s $^{-1}$  cm $^{-2}$  arcmin $^{-2}$  in 2–10 keV.

#### 4. DISCUSSION AND CONCLUSION

We have found extended X-ray emission around V4641 Sgr. The derived extension of  $\sim 20$  pc assuming a Gaussian-like radial profile is smaller than that seen in gamma rays ( $\approx 60$  pc with the HAWC observation: Alfaro et al. 2024). Here we first discuss the nature of the acceleration environment with an assumption that the X-rays are of non-thermal origin. Although we cannot confidently identify the exact site of particle acceleration, the X-ray radial profile describable with a Gaussian function centered at V4641 Sgr suggests that the acceleration site is close to the microquasar ( $\lesssim 10$  pc). The synchrotron cooling timescale for X-ray-emitting electrons is  $t_{\text{cool}} \approx 1000$  yr  $(E_e/100 \text{ TeV})^{-1} (B/10 \mu\text{G})^{-2}$ , where the  $E_e$  and  $B$  are the electron energy and magnetic field strength, respectively. The diffusion length for this timescale is  $R_{\text{dif}} \approx (4D(100 \text{ TeV})t_{\text{cool}})^{0.5} \approx 80$  pc  $(D(100 \text{ TeV})/5 \times 10^{29} \text{ cm}^2 \text{ s}^{-1})^{0.5} (E_e/100 \text{ TeV})^{-0.5} (B/10 \mu\text{G})^{-1}$ , where the  $D(E_e)$  is the diffusion coefficient. Thus, electrons with energies  $\approx 100$  TeV can travel within the X-ray emitting region, if we assume the Galactic mean value for  $D(E_e) = 2 \times 10^{28} \text{ cm}^2 \text{ s}^{-1} (E_e/3 \text{ GeV})^\delta$  with  $\delta = 0.3\text{--}0.6$  (Berezinskii et al. 1990; Ptuskin et al. 2006). To match the observed X-ray extent  $R_{\text{dif}} \approx 10$  pc, either an enhanced magnetic field  $B \approx 80 \mu\text{G}$  with  $D(E_e) = 2 \times 10^{28} \text{ cm}^2 \text{ s}^{-1} (E_e/3 \text{ GeV})^{0.3}$  or a suppressed diffusion coefficient  $D(100 \text{ TeV}) \approx 1 \times 10^{27} \text{ cm}^2 \text{ s}^{-1}$  with an interstellar magnetic field level  $B \approx 3 \mu\text{G}$  is required.

Given that the very-high-energy gamma-ray emission is likely hadronic due to the very hard spectra with  $\Gamma = 2.2 \pm 0.2$  (Alfaro et al. 2024; LHAASO Collaboration 2024), one can constrain the lower limit of the magnetic-field strength based on the highest allowed level of the inverse Compton gamma-ray flux. As shown in Figure 5, we obtain  $B \gtrsim 8 \mu\text{G}$ , which indicates that the magnetic field is likely enhanced compared with the interstellar values. Since the spectral shape of accelerated electrons is completely unknown, we assume a cutoff power-law model and have examined various parameter sets, with the index of 2–3 and the cutoff energy of 10–100 TeV. Radiation cooling is also taken into consideration, as the X-ray spectrum is extracted from the region extending beyond  $R_{\text{dif}}$  (Figures 2 and 3), where electrons may be affected by cooling. In conclusion, the choice of the parameters and the cooling effect does not significantly affect the lower limit of  $\approx 8 \mu\text{G}$ .

If the X-ray emission is of thermal origin, one can discuss the physical process which produced the thermal

<sup>7</sup> Total sky-background rate of  $\approx 70\%$  particle-background rate in 1.2–7.0 keV for radii of 5–15 arcmin, roughly corresponding to the source region.

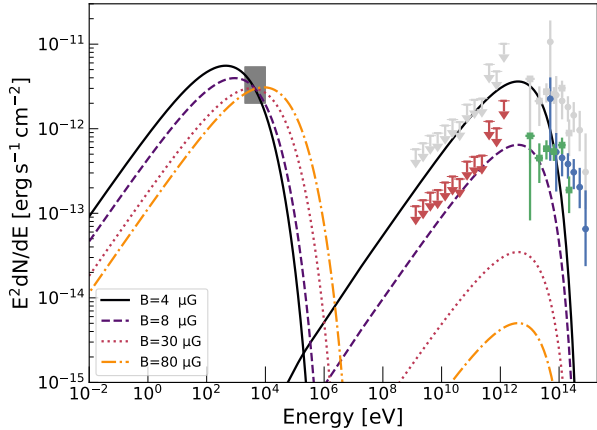


**Figure 5.** Broadband spectral energy distribution. The X-ray flux is derived for the XRISM source region (Figure 2 (a)). The red, green, and blue flux points indicate gamma-ray spectra by Fermi-LAT, HAWC, and LHAASO (Neronov et al. 2024; Alfaro et al. 2024; LHAASO Collaboration 2024), respectively, scaled to the XRISM source region, while the gray points show spectra from the entire gamma-ray emitting region. Synchrotron and inverse Compton models with various magnetic field strengths are overlaid, assuming electrons with a power-law index of 2 and a cutoff energy of 50 TeV. The total energy content in electrons ( $E > 1$  TeV) is  $2.6 \times 10^{47}$ ,  $4.7 \times 10^{46}$ ,  $2.5 \times 10^{45}$ , and  $3.6 \times 10^{44}$  erg for  $B = 4, 8, 30,$  and  $80 \mu\text{G}$ , respectively.

plasma based on the electron temperature and plasma density. Assuming a shock heating as a representative scenario to generate X-ray emitting plasma in interstellar space, the derived electron temperature  $\approx 3$  keV would require a shock velocity  $\gtrsim 1500$  km s $^{-1}$  (XRISM Collaboration 2024; Ohshiro et al. 2024). Plasma density  $\sim 0.3$  cm $^{-3}$  is typical for the interstellar medium. A supernova remnant would be able to explain these parameters, but the age estimate for the black hole in this system,  $\gtrsim 10$  Myr (Salvesen & Pokawanvit 2020), would contradict this scenario. Thus, a shock originating from black hole activities, e.g., a jet termination shock, would be more feasible. If we assume a pair of jets along the line-of-sight direction (Hjellming et al. 2000; Orosz et al. 2001), strong and adiabatic shock, and homogeneous plasma, the jet luminosity can be estimated from the shock kinetic energy as  $L_{\text{jet}} \sim 2 \times 10^{39}$  erg s $^{-1}$  ( $n_{\text{ISM}}/0.08$  cm $^{-3}$ )( $v_{\text{jet}}/1500$  km s $^{-1}$ ) $^3$ ( $R/10$  pc) $^2$ , where the  $n_{\text{ISM}}$ ,  $v_{\text{jet}}$ , and  $R$  are the interstellar plasma density, jet velocity, and radius of the extended emission, respectively. This is comparable to the Eddington luminosity of the system (MacDonald et al. 2014; Gandhi et al. 2019). This luminosity would not be unrealistic as the jet luminosity during the outburst in 1999 was inferred to exceed  $10^{39}$  erg s $^{-1}$  (Revnivtsev et al. 2002). The spatial extent of the lobe produced by the jet to

explain the observed extended X-rays,  $\gtrsim 20$  pc, would be much larger than the typical size of the radio lobes found in microquasars such as Circinus X-1, Cygnus X-1, and GRS 1758–258 ( $\lesssim 5$  pc; see a review by Gallo 2010), but would be comparable to the X-ray extension of the SS 433/W50 complex ( $\sim 30$  pc; Safi-Harb et al. 2022). Such a large spatial extent may be related to the inferred high jet luminosity. Alfaro et al. (2024) suggests that a jet with a luminosity of  $10^{39}$  erg s $^{-1}$  can, in principle, explain the extension of the TeV emission around V4641 Sgr ( $\approx 60$  pc).

An alternative origin to the extended X-ray emission around V4641 Sgr could be a dust scattering halo. The flux of the scattered photons can be evaluated based on the relation between an interstellar absorption column and optical depth in scattering (Predehl & Schmitt 1995), the absorption column density  $\approx 1.6 \times 10^{21}$  cm $^{-2}$ , and a typical flux of V4641 Sgr during the bursting activity from September 2024,  $\sim 10^{-11}$ – $10^{-10}$  erg s $^{-1}$  cm $^{-2}$ <sup>8</sup>. The resultant flux level for the source region,  $< 10^{-13}$  erg s $^{-1}$  cm $^{-2}$  in 2–4 keV, is lower than the sky background. We have also examined 25-ks archival Chandra data of V4641 Sgr in 2002 (ObsID: 3800), which were obtained during its quiescence ( $\sim$ five months after the outburst in May 2002) with a low flux of V4641 Sgr  $\sim 10^{-12}$  erg s $^{-1}$  cm $^{-2}$ <sup>9</sup>. With the same source and sky-background spectral models as the case (a) (Section 3.2) plus a particle-background model for Chandra ACIS (Suzuki et al. 2021), we obtained a surface brightness of the excess source,  $\sim 7 \times 10^{-15}$  erg s $^{-1}$  cm $^{-2}$  arcmin $^{-2}$  in 2–10 keV, similar to that obtained with XRISM. This supports the idea that the extended emission is more persistent and thus independent of the bursting activity of V4641 Sgr. To conclude, it is unlikely that the observed extended X-rays are due to dust scattering, without specific conditions such as the presence of dense clumps in the line of sight.

This work has discovered for the first time extended emission around V4641 Sgr with XRISM Xtend. The spatial extent of the X-ray emission  $\sim 20$  pc in diameter is smaller than that seen in gamma rays. Assuming that the X-rays are of non-thermal origin, this suggests that the X-rays originate from an electron population near the acceleration sites, which is different from that

<sup>8</sup> See, e.g., the report on MAXI/GSC observations in September 2024 (<https://www.astronomerstelegram.org/?read=16804>) and XRISM results by Shidatsu et al. in preparation.

<sup>9</sup> Note that this observation covered a limited region where one cannot obtain a background region free from the extended source according to the extension measured with XRISM. Thus it is hard to detect the extended emission with this Chandra observation alone.

responsible for the gamma-ray emission. If the X-rays are of thermal origin, a jet termination shock would be able to explain the measured properties with a jet luminosity  $\sim 2 \times 10^{39}$  erg s<sup>-1</sup>, which is comparable to the Eddington luminosity of this system. Future radio observations and more extensive X-ray observations of the gamma-ray emitting region will help disentangle the nature of the acceleration environment.

#### ACKNOWLEDGMENT

We appreciate the helpful suggestions by the anonymous referee, which have improved the quality of this paper. Part of this work was supported by

JSPS KAKENHI grant numbers 22KJ3059, 24K17093 (H.S.), 22K14064, 24H01819 (N.T.), 24K17105 (Y.K.), 22K14028, 21H04487, 23H04899 (S.S.K.), 19K14762, 23K03459, 24H01812 (M.S.), NSF award 2209533, the Tohoku Initiative for Fostering Global Researchers for Interdisciplinary Sciences (TI-FRIS) of MEXT's Strategic Professional Development Program for Young Researchers, the Inter-University Research Programme of the Institute for Cosmic Ray Research (ICRR), University of Tokyo, Grant 2024i-F-05, Marco Perez Cisneros and the offices of CUCEI, Universidad de Guadalajara for the financial support of the research stays at ICRR in 2023 and 2024, and the Spanish *Agencia estatal de investigaci'on* via PID2021-124879NB-I00.

#### REFERENCES

- Abeysekara, A. U., Albert, A., Alfaro, R., et al. 2018, *Nature*, 562, 82, doi: [10.1038/s41586-018-0565-5](https://doi.org/10.1038/s41586-018-0565-5)
- Alfaro, R., Alvarez, C., Arteaga-Velázquez, J., et al. 2024, *Nature*, 634, 557, doi: [10.1038/s41586-024-07995-9](https://doi.org/10.1038/s41586-024-07995-9)
- Arnaud, K. A. 1996, *Astronomical Society of the Pacific Conference Series*, Vol. 101, *XSPEC: The First Ten Years*, ed. G. H. Jacoby & J. Barnes, 17
- Berezinskii, V., Bulanov, S., Ginzburg, V., Dogiel, V., & Ptuskin, V. 1990, *Cosmic ray astrophysics* (Amsterdam: North Holland)
- Cash, W. 1979, *ApJ*, 228, 939, doi: [10.1086/156922](https://doi.org/10.1086/156922)
- Foster, A. R., Ji, L., Smith, R. K., & Brickhouse, N. S. 2012, *ApJ*, 756, 128, doi: [10.1088/0004-637X/756/2/128](https://doi.org/10.1088/0004-637X/756/2/128)
- Gallo, E. 2010, in *Lecture Notes in Physics*, Berlin Springer Verlag, ed. T. Belloni, Vol. 794, 85, doi: [10.1007/978-3-540-76937-8\\_4](https://doi.org/10.1007/978-3-540-76937-8_4)
- Gandhi, P., Rao, A., Johnson, M. A. C., Paice, J. A., & Maccarone, T. J. 2019, *MNRAS*, 485, 2642, doi: [10.1093/mnras/stz438](https://doi.org/10.1093/mnras/stz438)
- H. E. S. S. Collaboration, Aharonian, F., Ait Benkhali, F., et al. 2024, *Science*, 383, 402, doi: [10.1126/science.adi2048](https://doi.org/10.1126/science.adi2048)
- HEASARC. 2014, HEASoft: Unified Release of FTOOLS and XANADU. <http://ascl.net/1408.004>
- HI4PI Collaboration, Ben Bekhti, N., Flöer, L., et al. 2016, *A&A*, 594, A116, doi: [10.1051/0004-6361/201629178](https://doi.org/10.1051/0004-6361/201629178)
- Hjellming, R. M., Rupen, M. P., Hunstead, R. W., et al. 2000, *ApJ*, 544, 977, doi: [10.1086/317255](https://doi.org/10.1086/317255)
- Ishisaki, Y., Ezoe, Y., Yamada, S., et al. 2018, *Journal of Low Temperature Physics*, 193, 991, doi: [10.1007/s10909-018-1913-4](https://doi.org/10.1007/s10909-018-1913-4)
- Kuntz, K. D., & Snowden, S. L. 2008, *A&A*, 478, 575, doi: [10.1051/0004-6361:20077912](https://doi.org/10.1051/0004-6361:20077912)
- Kushino, A., Ishisaki, Y., Morita, U., et al. 2002, *PASJ*, 54, 327, doi: [10.1093/pasj/54.3.327](https://doi.org/10.1093/pasj/54.3.327)
- LHAASO Collaboration. 2024, arXiv e-prints, arXiv:2410.08988, doi: [10.48550/arXiv.2410.08988](https://doi.org/10.48550/arXiv.2410.08988)
- Loewenstein, M., Hill, R. S., Holland, M. P., et al. 2020, in *Proc. SPIE*, Vol. 11444, 114445D, doi: [10.1117/12.2560840](https://doi.org/10.1117/12.2560840)
- MacDonald, R. K. D., Bailyn, C. D., Buxton, M., et al. 2014, *ApJ*, 784, 2, doi: [10.1088/0004-637X/784/1/2](https://doi.org/10.1088/0004-637X/784/1/2)
- Masui, K., Mitsuda, K., Yamasaki, N. Y., et al. 2009, *PASJ*, 61, S115, doi: [10.1093/pasj/61.sp1.S115](https://doi.org/10.1093/pasj/61.sp1.S115)
- Mori, K., Tomida, H., Nakajima, H., et al. 2022, in *Proc. SPIE*, Vol. 12181, 121811T, doi: [10.1117/12.2626894](https://doi.org/10.1117/12.2626894)
- Mori et al. 2024, in *Space Telescopes and Instrumentation 2024: Ultraviolet to Gamma Ray*, ed. J.-W. A. den Herder, S. Nikzad, & K. Nakazawa, Vol. 13093, International Society for Optics and Photonics (SPIE), 130931I, doi: [10.1117/12.3019804](https://doi.org/10.1117/12.3019804)
- Nakajima, H., Maeda, Y., Uchida, H., et al. 2018, *PASJ*, 70, 21, doi: [10.1093/pasj/psx116](https://doi.org/10.1093/pasj/psx116)
- Neronov, A., Oikonomou, F., & Semikoz, D. 2024, arXiv e-prints, arXiv:2410.17608, doi: [10.48550/arXiv.2410.17608](https://doi.org/10.48550/arXiv.2410.17608)
- Ohshiro, Y., Suzuki, S., Okada, Y., Suzuki, H., & Yamaguchi, H. 2024, *The Astrophysical Journal*, 976, 180, doi: [10.3847/1538-4357/ad822d](https://doi.org/10.3847/1538-4357/ad822d)
- Orosz, J. A., Kuulkers, E., van der Klis, M., et al. 2001, *ApJ*, 555, 489, doi: [10.1086/321442](https://doi.org/10.1086/321442)
- Predehl, P., & Schmitt, J. H. M. M. 1995, *A&A*, 293, 889
- Ptuskin, V. S., Moskalenko, I. V., Jones, F. C., Strong, A. W., & Zirakashvili, V. N. 2006, *ApJ*, 642, 902, doi: [10.1086/501117](https://doi.org/10.1086/501117)
- Revnivtsev, M., Gilfanov, M., Churazov, E., & Sunyaev, R. 2002, *A&A*, 391, 1013, doi: [10.1051/0004-6361:20020865](https://doi.org/10.1051/0004-6361:20020865)

- Safi-Harb, S., Mac Intyre, B., Zhang, S., et al. 2022, *ApJ*, 935, 163, doi: [10.3847/1538-4357/ac7c05](https://doi.org/10.3847/1538-4357/ac7c05)
- Salvesen, G., & Pokawanvit, S. 2020, *MNRAS*, 495, 2179, doi: [10.1093/mnras/staa1094](https://doi.org/10.1093/mnras/staa1094)
- Suzuki, H., Plucinsky, P. P., Gaetz, T. J., & Bamba, A. 2021, *A&A*, 655, A116, doi: [10.1051/0004-6361/202141458](https://doi.org/10.1051/0004-6361/202141458)
- Tamura, K., Hayashi, T., Boissay-Malaquin, R., et al. 2022, in *Space Telescopes and Instrumentation 2022: Ultraviolet to Gamma Ray*, ed. J.-W. A. den Herder, S. Nikzad, & K. Nakazawa, Vol. 12181, International Society for Optics and Photonics (SPIE), 121811V, doi: [10.1117/12.2629534](https://doi.org/10.1117/12.2629534)
- Tamura et al. 2024, in *Space Telescopes and Instrumentation 2024: Ultraviolet to Gamma Ray*, ed. J.-W. A. den Herder, S. Nikzad, & K. Nakazawa, Vol. 13093, International Society for Optics and Photonics (SPIE), 130931M, doi: [10.1117/12.3020109](https://doi.org/10.1117/12.3020109)
- Tashiro, M., Maejima, H., Toda, K., et al. 2018, in *Society of Photo-Optical Instrumentation Engineers (SPIE) Conference Series*, Vol. 10699, Proc. SPIE, 1069922, doi: [10.1117/12.2309455](https://doi.org/10.1117/12.2309455)
- Tashiro, M., Maejima, H., Toda, K., et al. 2020, in *Proc. SPIE*, Vol. 11444, 1144422, doi: [10.1117/12.2565812](https://doi.org/10.1117/12.2565812)
- Tashiro et al. 2024, in *Space Telescopes and Instrumentation 2024: Ultraviolet to Gamma Ray*, ed. J.-W. A. den Herder, S. Nikzad, & K. Nakazawa, Vol. 13093, International Society for Optics and Photonics (SPIE), 130931G, doi: [10.1117/12.3019325](https://doi.org/10.1117/12.3019325)
- Terada, Y., Holland, M., Loewenstein, M., et al. 2021, *Journal of Astronomical Telescopes, Instruments, and Systems*, 7, 037001, doi: [10.1117/1.JATIS.7.3.037001](https://doi.org/10.1117/1.JATIS.7.3.037001)
- Uchiyama, H., Nobukawa, M., Tsuru, T. G., & Koyama, K. 2013, *PASJ*, 65, 19, doi: [10.1093/pasj/65.1.19](https://doi.org/10.1093/pasj/65.1.19)
- Wilms, J., Allen, A., & McCray, R. 2000, *ApJ*, 542, 914, doi: [10.1086/317016](https://doi.org/10.1086/317016)
- XRISM Collaboration. 2024, arXiv e-prints, arXiv:2408.14301, doi: [10.48550/arXiv.2408.14301](https://doi.org/10.48550/arXiv.2408.14301)
- Yamauchi, S., Nobukawa, K. K., Nobukawa, M., Uchiyama, H., & Koyama, K. 2016, *PASJ*, 68, 59, doi: [10.1093/pasj/psw057](https://doi.org/10.1093/pasj/psw057)
- Yeung, M. C. H., Ponti, G., Freyberg, M. J., et al. 2024, *A&A*, 690, A399, doi: [10.1051/0004-6361/202451045](https://doi.org/10.1051/0004-6361/202451045)